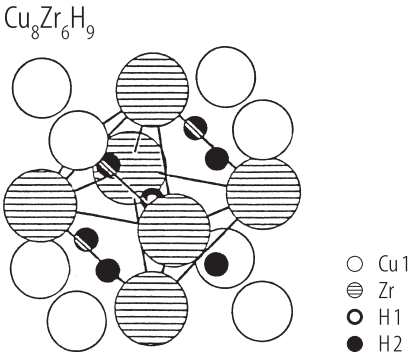

Fig. 51. $Cu_8Zr_6H_9$ subunit in the G hydride phase $Cu_{16}Zr_6Al_7H_x$ with its centre in the origin of the unit cell and the structural data for a composition with x = 8.2 [90M2]. Interatomic distances in pm:

H1-H2	190.5
H2-H2	220.0
H2-Cu1	173.1
H1-Zr	243.6
H2-Zr	205.0
Cu1-Zr	298.8
Cu1-Cu1	258.9
Al1-Cu1	246.6
Al1-Zr	307.0

1.5.5.2.6 Films/ribbons

The degree of atomic order can be influenced by preparing specimen in the form of ribbons or thin films. The crystallisation of amorphous Ni–Cu–Zr alloys has been investigated using X-ray and TEM techniques.

Table 14 indicates which elements are likely to form films with the Heusler structure.

Table 14. Formation of Heusler compounds for various compositions of X_2YZ. The plus sign refers to cases where alloying has led to the formation of the Heusler compound. The minus sign refers to cases where no Heusler compounds were found. A circle denotes systems for which Heusler phases are found experimentally over a broad temperature range and at normal pressure [87K3].

(**a**) Heusler compound Co_2YZ.

Y	Z								
	Al	Si	Ga	Ge	In	Sn	Sb	Tl	Pb
Li			+			+			
Be	+	⊕	+		+	+	+	+	+
Mg			+	⊕		+			
K		+	–	–	–	+	–	–	–
Sc		+	–	–	–	+	–	–	–
Ti	⊕	+	⊕	⊕	+	⊕	+	+	+
V	+	⊕	⊕	+	+	⊕	+	+	+
Cr	+	+	⊖			+			
Fe	⊕	⊖	–	–		+			
Ni			–	–	–	+	⊖	–	–
Y			+		–	+	–	–	–
Zr	⊕	+				⊕			
Nb	⊕	+				⊕			
Mo	+	+	+			+			
Ru	+	+	+			+			
Rh			+		–	+	–	–	–
Pd			+		–	+	–	–	–
Ag			+		–	+	–	–	–
Lu	+	+	+		+	+	+		
Hf	⊕	+	+	+	+	⊕	+		
Ta	⊕	+	⊕	+	+	+	+		
Au	+	+	+		+	+	+		

(**b**) Heusler compound Ni_2YZ.

Y	Z								
	Al	Si	Ga	Ge	In	Sn	Sb	Tl	Pb
Li		–			+	+	+		
Be		–			+	+	+		
Mg			+	+	⊕	⊕	⊕	+	+
K	+				+	+	+		
Sc	⊕		⊕	+	+	+	+		
Ti	⊕		⊕	+	⊕	⊕	⊕		
V	⊕		⊕		+	⊕	+		
Cr	⊖		⊖		+	+	+		
Mn	+	+	⊕	⊕	⊕	⊕	⊕	+	+
Fe	+		+		+	+	+		
Co	+				+	+	+		
Zn	+	+	+	+	+	+	+	+	+
Y	+						+		
Zr	⊕		⊕		⊕	⊕	+		
Mo	+				–	–		–	–
Ru	+				–	–		–	–
Rh	+				–	–		–	–
Lu	+	+	+					+	+
Hf	⊕	+	⊕	+	⊕	⊕		+	+
Ta	⊕	+	⊕	+				+	+
Au	+	+	+		+	+	+		

(**c**) Heusler compound Pd_2YZ.

Y	Z								
	Al	Si	Ga	Ge	In	Sn	Sb	Tl	Pb
Li			+	⊕	⊖	⊖			
Be			+		–				
Mg			+		+				
K			+		–				
Sc	+	+	+		⊕				
Ti	⊕	+	+		⊕				
V	+	+	+		–				
Cr			+			+	+	+	+
Mn	+	+	+	⊕	⊕	⊕	⊕	+	+
Fe	+	+	+	+					
Ni	+		⊖	–	–	–	–	–	–
Zn	+	+	+		–				
Y	+	+	+		⊕	+	⊕	+	⊕
Zr	⊕	+		–	⊕				
Nb	+	+		–					
Mo	+	+		–	+				
Ru	+	+		–	+				
Rh	+	+		–					

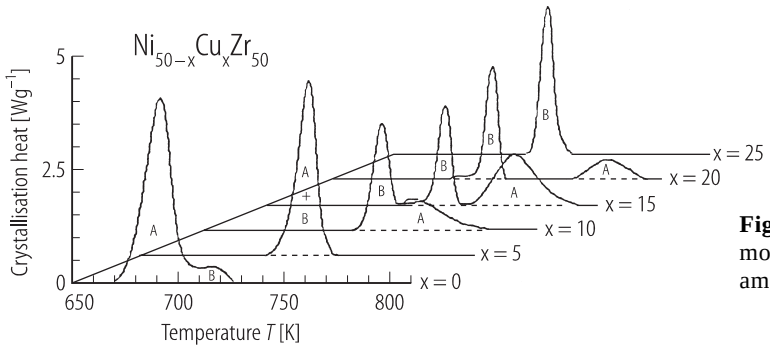

Fig. 52. 10 K/min crystallisation thermograms of six different $Ni_{50-x}Cu_xZr_{50}$ amorphous alloys [92G1].

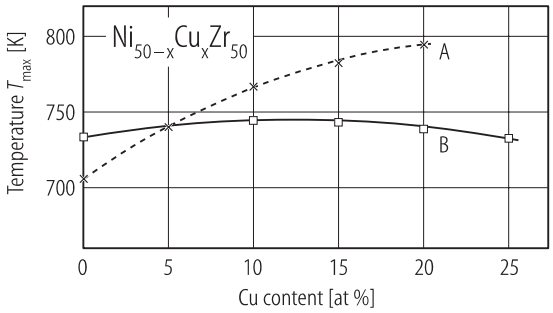

Fig. 53. $Ni_{50-x}Cu_xZr_{50}$. Peak temperatures of the A and B sub-peaks vs. the Cu concentration (heating rate = 20 K/min) [92G1].

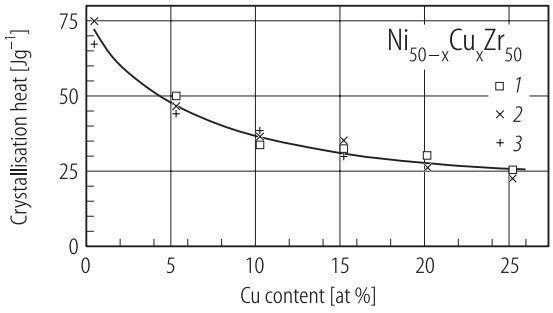

Fig. 54. $Ni_{50-x}Cu_xZr_{50}$. Heat of crystallisation plotted as a function of the Cu content [92G1]. Heating rates: *1* 40 K/min, *2* 20 K/min, *3* 10 K/min.

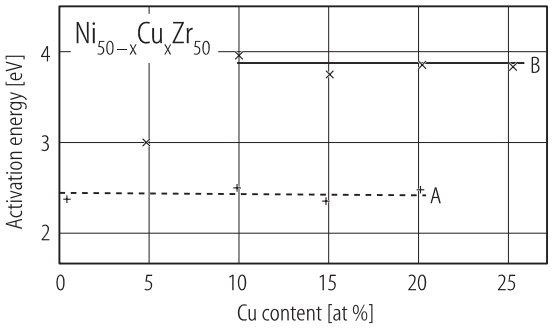

Fig. 55. $Ni_{50-x}Cu_xZr_{50}$. Activation energies of peaks A and B vs. the Cu concentration [92G1].

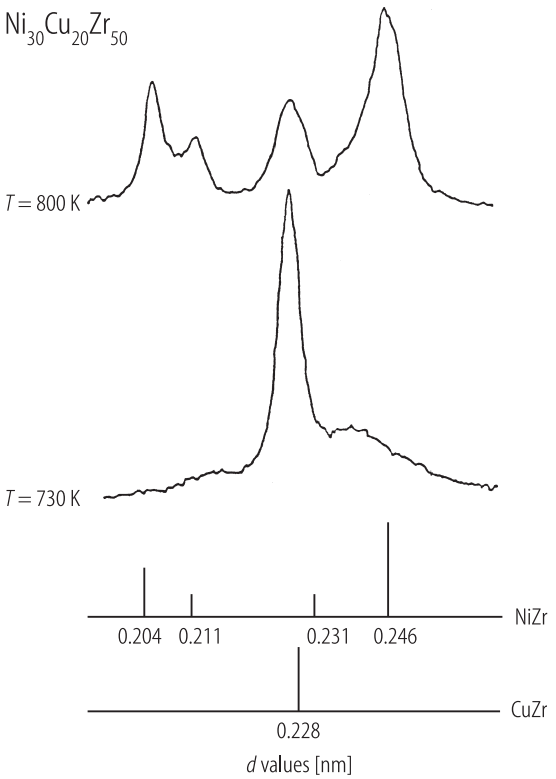

Fig. 56. $Ni_{30}Cu_{20}Zr_{50}$. X-ray intensity distribution of the 20 at% Cu sample heated up to the end of peak B (730 K) and A (800 K), respectively [92G1]. *d*: lattice spacing.

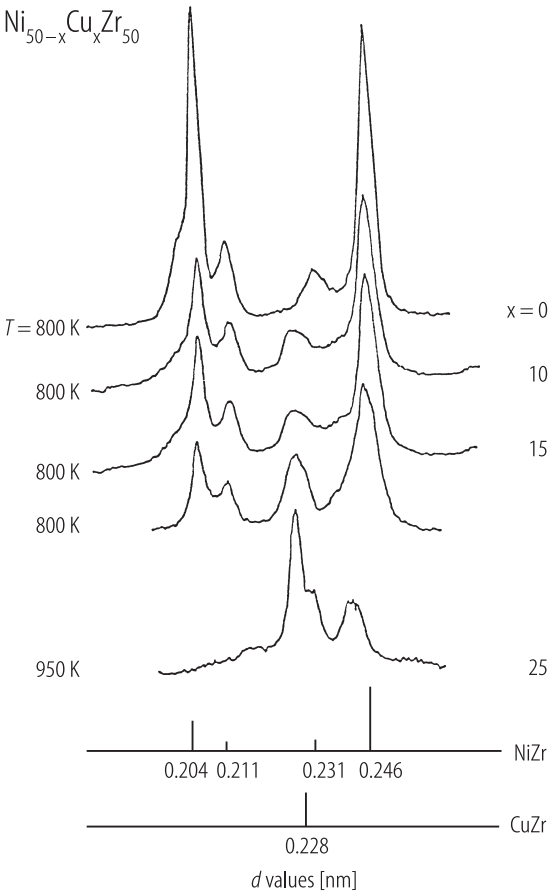

Fig. 57. $Ni_{50-x}Cu_xZr_{50}$. X-ray curves of the samples heated up to the temperatures indicated [92G1]. *d*: lattice spacing.

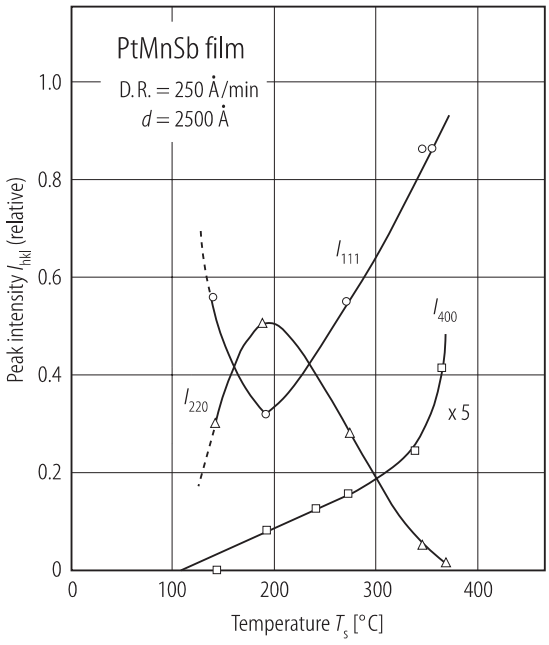

Fig. 59. Dependence of relative peak intensity on substrate temperature. (D.R: deposition rate; *d*: film thickness) [88N3].

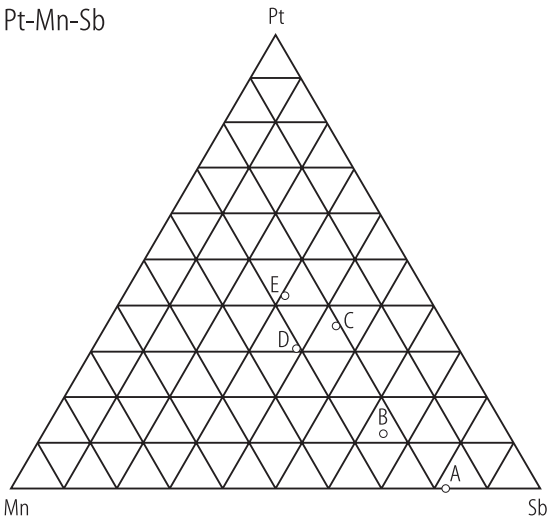

a

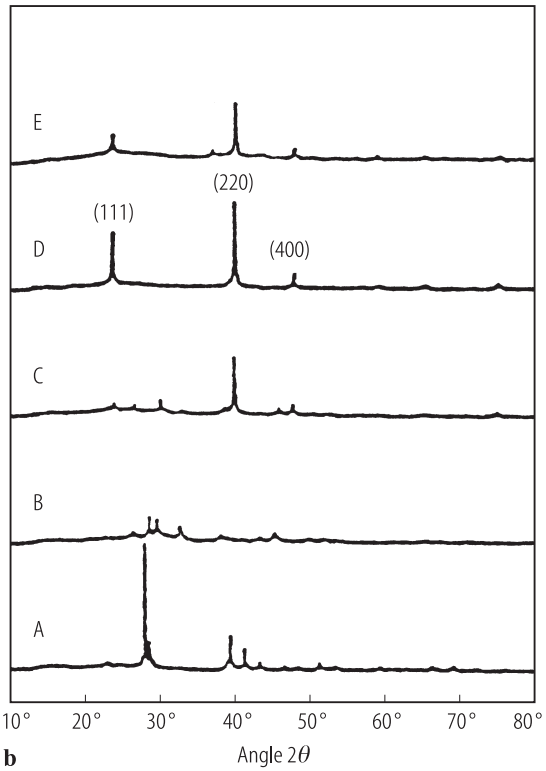

b

Fig. 58. X-ray diffraction patterns for various PtMnSb compositions: (**a**) compositional diagram; (**b**) diffraction pattern [88N3].

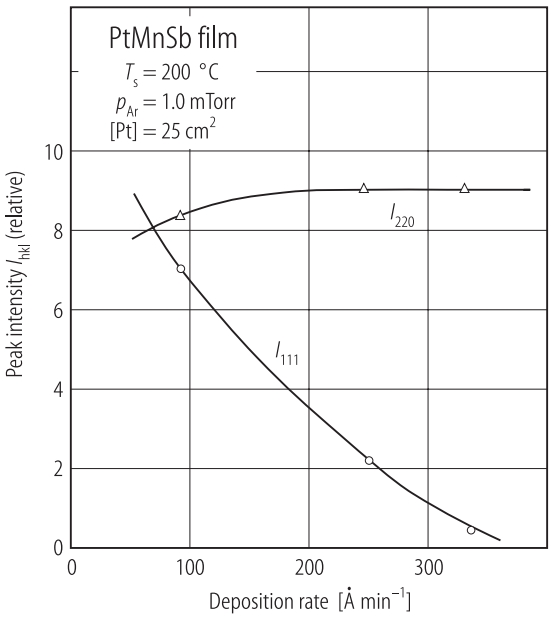

Fig. 60. Diffraction peak intensity as a function of deposition rate at argon pressure p_{Ar} = 1.0 mTorr (Pt: area of Pt chips) [88N3].

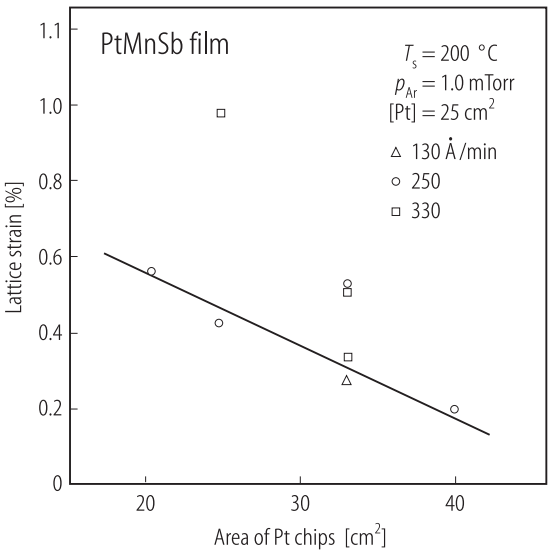

Fig. 61. Lattice strain (1 – *c*/*a*) vs. area of Pt chips in PtMnSb films for various deposition rates [88N3].

1.5.5.3 Bulk magnetic properties

1.5.5.3.1 Introduction

The investigation of the bulk magnetic properties of materials is an essential first step in obtaining an understanding at a microscopic level. Frequently analysis of these data is made, particularly for ferromagnetic materials, using Arrott plots in which the data is presented in the form of M^2 versus B/M isotherms. From these isotherms it is possible to ascertain whether a material has a spontaneous moment, the Curie temperature, the degree of magnetic homogeneity etc. However the application of Arrott plots is not restricted to ferromagnetic materials and in view of the information which may be obtained from such analysis and its importance to the present review a detailed account is given below.

1.5.5.3.2 Arrott plots

1.5.5.3.2.1 Introduction

The use of Arrott plots to analyse bulk magnetic properties arises from the application of Landau theory. It is the notion of an order parameter and the fact that the symmetry of the system can be treated exactly that makes this approach particularly attractive [90I1, 87T1]. By using an expansion of the free energy in powers of the order parameter (e.g. the ferromagnetic moment or the staggered magnetisation in an antiferromagnet) the magnetic behaviour may be described using a small number of (temperature dependent) coefficients. These coefficients may be extracted from experimental observations of the magnetic moment as a function of external field and temperature with the help of Arrott plots, namely M^2 vs. $\mu_0 H/M$. For a ferromagnetic system this can be readily obtained from measurements of the magnetisation.